JOURNAL OF GEOPHYSICAL RESEARCH, VOL. 105, NO. E1, PAGES 1685–1694, JANUARY 25, 2000

Quantifying groundwater-sapping landforms with a hypsometric technique

Wei Luo

Department of Geography, Northern Illinois University, DeKalb

Abstract. The groundwater-sapping process generates peculiar landform features, including amphitheater channel head, U-shaped cross section with steep wall and flat floor, and short stubby tributaries. However, previous attempts to quantify this landform were primarily limited to the planform geometry of the channel networks and the network topology. The elevation or relief information, which is more revealing of the processes that gave rise to the landform, has not received enough attention in the literature. The hypsometric curve (area-altitude relation) combines area and relief elegantly. By treating the hypsometric curve as a probability distribution, one can quantitatively distinguish small differences in the shape of the curve (and thus in the characteristics of the landform) on the basis of hypsometric integral, the skewness and kurtosis of the curve, and the skewness and kurtosis of its density function. Preliminary results of applying this technique within an automated Geographic Information System (GIS) environment to typical terrestrial sapping landforms show that they are characterized by high hypsometric integral, low hypsometric skewness, negative density skewness, and high density kurtosis as compared with typical fluvial landforms in humid regions. Statistical analyses indicate that the differences on these hypsometric attributes between typical sapping and typical terrestrial fluvial landforms are statistically significant. Thus the hypsometric analysis technique and hypsomtric attributes can be used to quantify landforms. This technique, along with other lines of evidence, can be applied to help identify the origin of landforms on other planets such as Mars, where groundwater-sapping is thought to have played an important role in its landform evolution.

1. Introduction

Groundwater-sapping is defined by *Laity and Malin* [1985, p.203] as "the process leading to the undermining and collapse of valley head and side walls by weakening or removal of basal support as a result of enhanced weathering and erosion by concentrated fluid flow at a site of seepage" (Figure 1). The characteristics of landforms produced by the groundwater-sapping process include theater-shaped head, near constant valley width from source to outlet, high and steep valley sidewalls, valley network controlled by structure, and low drainage density [*Laity and Malin*, 1985]. Research on the groundwater-sapping and subsurface processes has been revived by attempts to interpret the landforms on Mars [*Jones*, 1997], where the aforementioned characteristics are found in its valley networks and are thought to be formed by the groundwater-sapping process [*Higgins*, 1982, 1984; *Baker*, 1982; *Howard et al.*, 1988]. The lack of dissected areas between valleys on the latest high-resolution Mars Orbiter Camera (MOC) images suggests erosion by water from a subsurface source (groundwater sapping) rather than from an atmospheric source (precipitation and fluvial erosion) [*Malin and Carr*, 1999]. However, there is also evidence, such as a well-integrated network at 26°S, 84°W, suggesting surface runoff [*Carr*, 1999]. In addition, the climatic conditions needed for valley formation, for river flow, and for recharging the groundwater table are still uncertain. The alternative explanation for a recharging groundwater system is hydrothermal circulation [e.g., *Gulick and Baker*, 1989, 1990; *Gulick*, 1998]. There is still no consensus, and the different geomorphic processes invoked to explain the landform also have different implications for past Martian climates [*Squyres and Kasting*, 1994]. The author believes that quantifying the landforms is an important step toward fully understanding the processes [*Lane et al.*, 1998] and is also important for quantitative modeling of the processes. Thus the objectives of this paper are to apply the hypsometric technique to quantify typical groundwater-sapping and fluvial landforms that are known and documented by fieldwork on Earth, to examine their hypsometric attribute values, and to determine whether such values are significantly different between the two groups of landforms. It is the hope of the author that this technique can be applied to Mars, along with other evidence and information (e.g., computer modeling and rover field observation), to help identify the forms and understand the processes that are responsible for these peculiar landforms using the high-resolution Mars Obiter Laser Altimeter (MOLA) data of Mars Global Surveyor (MGS).

Paper number 1999JE001096.
0148-0227/00/1999JE001096$09.00

2. Previous Work and the Hypsometric Technique

Previous studies on groundwater-sapping on Earth include the field investigation in Colorado Plateau by *Laity and Malin*

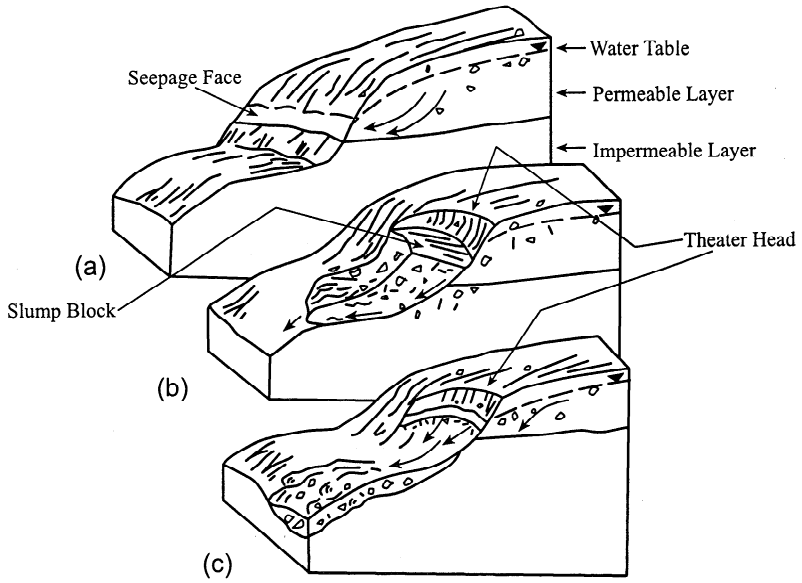

Figure 1. Schematic block diagram showing the groundwater-sapping process. (a) Groundwater in the permeable layer seeps out as springs at the seepage face, causing weakening of the impermeable (often friable, e.g., shale) layer and (b) subsequent undermining and slumping of the overlying layer. (c) This process typically forms amphitheater channel head and slumped blocks. Figure adapted after *Coates* [1990].

[1985], the flume experiment and computer modeling by *Howard* [1988], and the planform quantification by *Kochel and Piper* [1986] of the valleys on the Hawaii Islands. In 1990, the Geological Society of America published a collection of papers on groundwater geomorphology that summarized the advances in this field [*Higgins and Coats*, 1990]. Recently, a number of researchers have reported the groundwater-sapping landforms in Massachusetts, Florida, England, Japan, and Egypt [e.g., *Uchupi and Oldale*, 1994; *Schumm et al.*, 1995; *Nash*, 1996; *Onda*, 1994; *Luo et al.*, 1997]. The sapping process is better understood, at least qualitatively, than before, but research on how to quantitatively identify this peculiar landform is still limited. The *Kochel and Piper* [1986] work was mostly concentrated on planform geometry, using parameters such as basin shape, basin area, drainage density, stream frequency, and basin area/canyon area ratio. The reason for this is that at that time the resolution of topographic data for Mars was very poor and researchers had to rely on planform information from remote-sensing images to interpret Martian landforms. As more detailed topographic data from Mars Global Surveyor are becoming available, it is possible and necessary to explore ways to incorporate information on the third dimension into landform interpretation. This paper demonstrates such an approach to quantify groundwater-sapping landforms using a hypsometric technique, which combines area and relief information and provides an alternative means to quantify landforms.

The hypsometric technique was first proposed by *Harlin* [1978] on the basis of hypsometric curve of a watershed basin, which describes the area-altitude relation or the distribution of area with elevation (Figure 2) [*Langbein*, 1947; *Strahler*, 1952]. Basically, this technique treats the hypsomtric curve as a cumulative probability distribution and uses statistical moments to describe the curve quantitatively [*Harlin*, 1978]. The hypsometric curve can be represented by a polynomial function, and its statistical moments can be derived mathematically in terms of the coefficients of the polynomial function [*Harlin*, 1978]. Since the hypsometric curve also represents an overall slope of the basin, the statistical moments can thus distinguish differences between basins. However, before the Geographic Information System (GIS) and the development of an automated procedure, hypsometric curves were obtained by measuring the areas between contour lines on a paper map manually or using an instrument [*Coradini et al.*, 1980], which was a tedious, time-consuming, and error-prone process and hindered the wide application of hypsometric analysis. With the advances in GIS and ready availability of digital topography data nowadays, the process of obtaining the curve and calculating its statistical attributes has been automated [*Luo*, 1998] (code available at http://www.iamg.org). It is now practical to use this technique to quantify landforms.

The statistical attributes in the hypsometric technique include hypsometric integral (INT), skewness of the hypsometric curve (hypsometric skewness, SK), kurtosis of the hypsometric curve (hypsometric kurtosis, KUR), skewness of the hypsometric density function (density skewness, DSK), and kurtosis of the hypsometric density function (density skewness, DKUR). The definitions of each term used in this paper are given below (please refer to *Harlin* [1978] for derivation on expressing these attributes in terms of polynomial coefficients):

$$\text{Hypsometric integral INT} = \iint_R dxdy\,, \tag{1}$$

where R is the region under the hypsometric curve, x is relative area, and y is relative height.

$$\text{Hypsometric skewness SK} = \frac{\mu_{30}}{(\mu_{20}^{1/2})^3}\,, \tag{2}$$

where μ_{30} is the third-order moment about x,

$$\mu_{30} = \frac{1}{\text{INT}}\iint (x-\mu_{10})^3\,dydx\,, \tag{3}$$

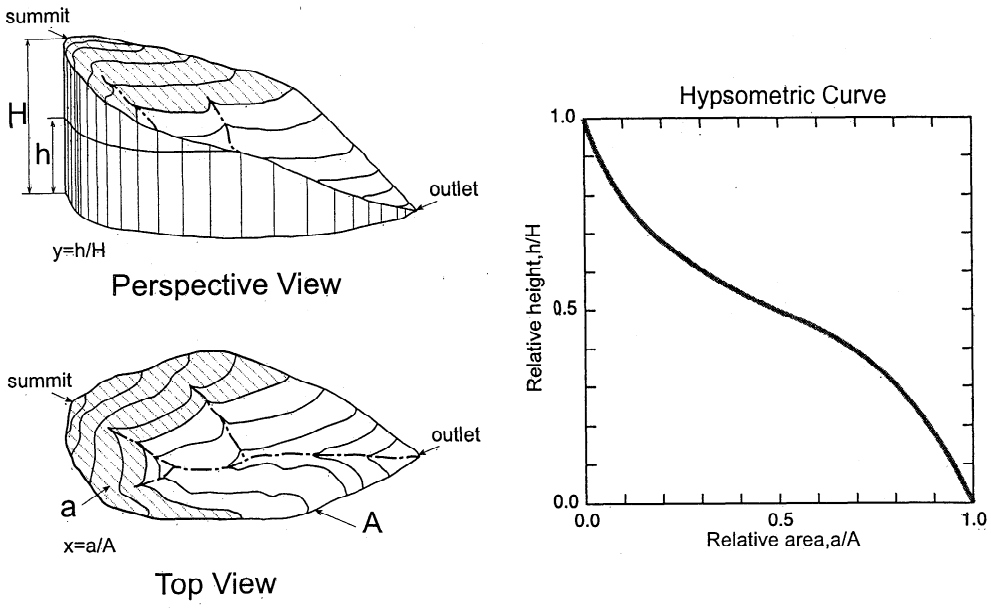

Figure 2. Schematic diagram illustrating the hypsometric curve and the variables involved. The curve essentially describes the distribution of area with elevation, i.e., the relative proportion of a region's area that lies at or above a given height relative to the total elevation range in the area under consideration (a, area of basin above height h; h, height above outlet; A, total area of basin; H, total relief of basin). Figure adapted after *Strahler* [1952].

where μ_{10} is the first-order moment or x mean or x centroid,

$$\mu_{10} = \frac{1}{\mathrm{INT}} \iint_R x\,dy\,dx, \tag{4}$$

and μ_{20} is the second-order moment about x or variance,

$$\mu_{20} = \frac{1}{\mathrm{INT}} \iint (x - \mu_{10})^2\,dy\,dx. \tag{5}$$

$$\text{Hypsometric kurtosis KUR} = \frac{\mu_{40}}{(\mu_{20}^{1/2})^4}, \tag{6}$$

where μ_{40} is the fourth-order moment about x,

$$\mu_{40} = \frac{1}{\mathrm{INT}} \iint (x - \mu_{10})^4\,dy\,dx. \tag{7}$$

Density skewness (DSK) and density kurtosis (DKUR) are defined similarly except that now y is the first derivative of the hypsometric curve, i.e., the density function of the hypsometric curve (replacing y with y'). These definitions are chosen so that they are consistent with Harlin's original work [*Harlin*, 1978].

In statistics, skewness and kurtosis describe the shape of a distribution relative to the normal distribution and are dimensionless. Skewness characterizes the degree of asymmetry of a distribution around its mean. A positive value of skewness signifies a distribution with an asymmetric tail extending out toward a more positive x (skewed to the right); a negative value signifies a distribution whose tail extends out toward a more negative x (skewed to the left). Kurtosis measures the relative peakedness or flatness of a distribution, relative to a normal distribution. Larger kurtosis (>3) indicates a "sharper" peak than normal distribution (under the definition used in this paper, the kurtosis of a normal distribution is 3); smaller kurtosis indicates "flatter" peak than normal distribution. According to *Harlin* [1978, 1984], the hypsometric skewness represents the amount of headward erosion in the upper reach of a basin; density skewness indicates slope change; a large value of kurtosis signifies erosion on both upper and lower reaches of a basin, and density kurtosis delineates midbasin slope. The integral of the curve (i.e., the area under the curve) portrays the amount of material left after erosion [*Strahler*, 1952]. All of these five variables will be referred to as hypsometric attributes, parameters, or variables in this paper. As typical groundwater-sapping is essentially headward erosion started at the lower reaches of the basin by emerging groundwater, it is expected that the hypsometric curve of a typical groundwater-sapping landform would have attributes characterized by high hypsometric intergral, low hypsometric skewness, negative density skewness, and high density kurtosis as compared with those of fluvial landforms in humid regions. Figure 3 schematically shows how the values of the skewness and density skewness relate to the shape of the hypsometric curve and thus to the characteristics of the landform.

3. Data Source

Seven and a half (7.5) minute digital elevation model (DEM) data were downloaded from the United States Geological Survey (USGS) via the Internet and were converted to the GRID format of Arc/Info GIS software. Once in GRID format, adjacent DEMs were mosaicked together because some watersheds span across several quadrangles. Next, hydrologic functions within the GRID system were used to automatically delineate the watershed boundaries [*Environmental Systems Research Institute*, 1993]. Forty-five watersheds were selected from areas where typical groundwater-sapping and fluvial landforms exist, and the

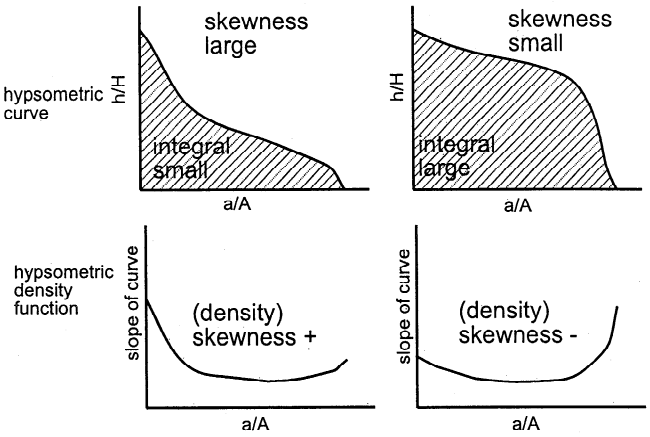

Figure 3. Schematic diagram showing the relationship between the shape of the hypsometric curve and its integral, skewness, and density skewness. The two left plots are typical for fluvial landform, and the two right plots are typical for sapping landform.

automated hypsometric technique [*Luo*, 1998] was applied to them to obtain their hypsometric attributes (Table 1). Twenty-five of the selected watersheds are from areas in Utah and Florida where the groundwater-sapping process was reported to be dominant on the basis of detailed field work [*Laity and Malin*, 1985; *Schumm et al.*, 1995]. Twenty of the watersheds are typical fluvial landforms from the unglaciated areas in Oklahoma, Iowa, and Wisconsin [*Harlin*, 1982; *Bridges*, 1990]. Two additional test basins were also obtained from Alabama and Mars (Table 1).

4. Results

In this section, typical hypsometric curves of groundwater-sapping and fluvial landforms and their corresponding attributes (skewness, kurtosis, density skewness, density kurtosis, and integral) obtained from the automated procedure are presented and discussed. This is followed by statistical tests and analyses that show the significant differences on hypsometric attributes between typical sapping and fluvial landforms. The statistical analyses was completed in SAS [*SAS Institute Inc.*, 1990].

Figure 4 shows typical fluvial and sapping landforms and their corresponding hypsometric curves along with their hypsometric attributes. The curve for the sapping landform is more convex upward in the middle to lower portion of the curve, indicating more erosion in the lower reach of the basin, whereas that for fluvial landform is more concave upward in the middle to upper portion of the curve, indicating more erosion in the upper reach of the basin. This is consistent with what one would expect on the basis of the definitions of the two processes. When the attribute data are graphed in scatterplots (Figure 5), one can see that the hypsometric attributes can generally separate the two landforms. These plots are much better than the principal component analysis (PCA) plots of *Kochel and Piper* [1986] because there is virtually no direct overlap of points. However, the ranges of values in kurtosis and density kurtosis do overlap between the two groups (Figures 5a, 5c-5f, 5h, and 5j), which suggests that kurtosis and density kurtosis are not as sensitive to the differences between the forms of the two landform groups as the other three attributes. Also, there is some correlation between kurtosis and skewness (Figure 5a) and between density kurtosis and density skewness (Figure 5f). Thus ignoring kurtosis and density kurtosis in discriminant analysis later should cause little harm to the effectiveness of this technique's ability to separate the two groups. The variable that is most effective in separating the forms of the two groups is density skewness (Figures 5b, 5d, and 5f).

In order to confirm the above qualitative observations from simple scatterplots, statistical *t* tests were conducted. The null hypothesis is that the means of the variables for typical sapping and typical fluvial groups are the same, and the alternative hypothesis is that they are different.

The statistics in Table 2 shows that differences of all variables between the two groups are statistically significant (at a confidence level of >95%) whether their variances are equal or not. The differences of skewness, density skewness, and hypsometric integral are highly statistically significant (at a confidence level of >99%). Thus we can safely reject the null hypothesis and accept the alternative hypothesis that the forms of the two landform groups are indeed different on the basis of these parameters. Table 2 also shows that for typical fluvial landforms the mean skewness is higher and the mean integral is lower than their counterparts for typical sapping landforms. This is because the typical sapping process starts at the lower reach of the basin and works its way up, leaving much of the upper reach areas uneroded and resulting in a less skewed hypsometric curve and a higher hypsometric integral. The opposite is true for the typical fluvial landform, which is eroded from the top down. The mean density skewness for the typical sapping landform is negative, whereas that for the typical fluvial landform is positive. This is because the density skewness describes the slope change. The typical sapping process starts at the lower reach of the basin and thus has more slope change there, which makes the density function negatively skewed (to the left) (Figure 3). The mean density kurtosis, which describes the midbasin slope, for the typical fluvial landform is smaller than that for the sapping landform. This is because typical fluvial process tends to smooth the midbasin slope, whereas the typical sapping process tends to steepen the midbasin slope. The kurtosises for the two landforms are different, but the differences are the least statistically significant among all variables (Table 2), which is consistent with the observation from the scatterplots.

Principal component analysis was also conducted to see which variables are more important in identifying and differentiating the two groups of landforms, i.e., to select a small set of variables that are almost as powerful as using all the variables to separate the two groups. The first two principal components can explain about 94% of the variance (Table 3). The loadings show that the first component (60% of the variance) is primarily, in the order of decreasing importance, density skewness, hypsometric integral, and skewness, whereas the second component is primarily density kurtosis and kurtosis (Table 3). This result is consistent with that of the *t* test analysis.

Finally, discriminant analyses were conducted, and results show that using all variables and using only the three highly significant variables (i.e., density skewness, integral, and skewness) led to the same error rate of separating the two groups. The linear discriminant functions using the three highly significant variables are as follows:

Table 1. Hypsometric Attributes for Fluvial and Sapping Landforms

	INT	SK	DSK	KUR	DKUR	DD	Relief	Area	Quadrangle(s) Watershed resides	State
F1	0.4666	0.3407	0.0659	1.9672	1.3202	1.7820	95.40	83.85	Platteville, Belmont	IA
F2*	0.5587	0.3369	-0.2770	2.0227	1.5296	1.9292	70.41	5.19	Zwingle	IA
F3	0.4914	0.3662	-0.0661	2.0240	1.3963	1.8744	64.92	5.18	Zwingle	IA
F4	0.4911	0.4432	-0.0026	2.1341	1.5048	1.7864	59.44	5.30	Zwingle	IA
F5	0.4865	0.3666	-0.0074	2.0139	1.3719	1.7806	68.28	7.70	Zwingle, La Motte	IA
F6	0.3629	0.3695	0.3716	1.9268	1.3867	1.8454	157.28	109.14	Anadarko E, Cyril	OK
F7	0.3791	0.4636	0.2345	2.0757	1.4194	1.9213	143.87	188.11	Anadarko NW, Cogar	OK
F8	0.4584	0.3676	0.0678	1.9991	1.3476	1.8361	114.30	69.10	Anadarko W, Anadarko E, Apache, Cyril	OK
F9	0.4027	0.3252	0.2253	1.9110	1.2917	1.9226	122.53	167.99	Cyril, Fletcher, Aparche	OK
F10	0.4726	0.3441	0.0089	1.9798	1.3296	1.7556	100.28	33.63	E Ninnekah, Rush Springs	OK
F11	0.4597	0.4331	0.1281	2.0886	1.4513	1.7322	109.12	30.65	E Ninnekah, Rush Springs	OK
F12	0.5090	0.3897	-0.0778	2.0600	1.4398	1.8259	73.15	16.27	E Roaring Rreek	OK
F13	0.4130	0.4175	0.2319	2.0344	1.4118	1.6789	142.95	84.92	Laverty	OK
F14	0.3514	0.4998	0.4485	2.0953	1.5659	1.8468	103.63	35.29	Laverty, Rock Ford	OK
F15	0.4684	0.3785	-0.0153	2.0317	1.3910	1.8500	66.14	35.45	Rush Springs	OK
F16	0.3642	0.5506	0.2575	2.2018	1.5952	1.8988	101.50	67.23	Verden	OK
F17	0.3907	0.5057	0.3554	2.1392	1.5385	1.8349	90.53	25.07	Verden	OK
F18	0.3830	0.5116	0.2128	2.1758	1.5026	1.8060	79.55	40.33	Verden, Chickasha, Laverty	OK
F19*	0.5752	0.2405	-0.3365	1.9210	1.4092	1.8332	96.93	117.00	Calamine, Belmont, Darlington, Shullsburg	WI
F20	0.4464	0.2542	0.1985	1.8484	1.2160	1.7888	83.21	35.04	Shullsburg	WI
S1	0.7014	0.2249	-1.0511	1.9744	2.8200	1.5544	56.39	12.62	Holt	FL
S2	0.6337	0.3418	-0.5994	2.0782	2.1003	1.3594	49.68	7.58	Holt	FL
S3	0.5210	0.3280	-0.2955	2.0114	1.5149	1.7269	82.60	108.72	Mossy Head, Niceville SE	FL
S4	0.5232	0.3515	-0.2149	2.0319	1.4902	1.7471	66.14	41.06	Niceville	FL
S5	0.5560	0.2833	-0.3331	1.9598	1.4566	1.6882	73.15	72.64	Niceville, Valparaiso	FL
S6	0.5602	0.3039	-0.2820	1.9825	1.4782	1.8191	53.04	17.10	Spencer	FL
S7	0.5207	0.3014	-0.3331	1.9779	1.4808	1.6570	75.59	69.23	Valparaiso	FL
S8	0.5560	0.2681	-0.4418	1.9596	1.5680	1.7025	57.00	19.73	Crestview S	FL
S9	0.5656	0.3099	-0.4200	2.0045	1.6215	1.5925	58.83	21.27	Crestview S	FL
S10	0.5424	0.2664	-0.4374	1.9563	1.5536	1.8648	56.69	61.26	Holt SW	FL
S11	0.5058	0.3565	-0.3080	2.0283	1.5468	1.6835	111.25	9.87	Alcove Canyon	UT
S12	0.5161	0.1849	-0.0973	1.8354	1.1478	1.9811	130.15	27.07	Alcove Canyon	UT
S13	0.5388	0.3269	-0.2238	2.0019	1.4616	1.9413	156.67	34.29	Alcove Canyon, Nokai Dome	UT
S14	0.5593	0.2403	-0.5699	1.9403	1.6759	1.8500	131.06	71.53	Alcove Canyon, The Rincon	UT
S15*	0.5139	0.3546	-0.0532	2.0095	1.3890	1.7954	129.24	16.03	Davis Gulch, Stevens Canyon S, Rincon	UT
S16	0.6387	0.3114	-0.6369	2.0387	2.0772	1.9371	155.45	39.61	Rincon NE	UT
S17	0.5451	0.3271	-0.0596	1.9806	1.3837	1.6620	179.53	11.05	Stevens Canyon N, Scorpion Gulch	UT
S18	0.6295	0.3179	-0.3508	2.0118	1.6373	1.6580	172.52	7.67	Stevens Canyon N, Stevens Canyon S	UT
S19	0.5966	0.3388	-0.5106	2.0599	1.8790	1.7719	171.30	27.73	Stevens Canyon S	UT
S20	0.6185	0.2181	-0.4578	1.9152	1.5092	1.7725	153.62	10.64	Stevens Canyon S	UT
S21	0.5781	0.4110	-0.2533	2.1355	1.7320	1.7536	133.81	4.49	Stevens Canyon S	UT
S22	0.5806	0.2419	-0.1156	1.9000	1.2899	1.7829	135.64	11.90	Stevens Canyon S	UT
S23	0.5058	0.2132	-0.3953	1.8519	1.3775	1.3798	122.22	6.00	Stevens Canyon S, Davis Gulch	UT
S24	0.5161	0.2762	-0.0142	1.9121	1.2653	1.8460	281.03	67.81	Stevens Canyon S, North	UT
S25	0.6091	0.2469	-0.3219	1.9289	1.4456	1.8308	147.22	12.91	Stevens Canyon S, Rincon NE	UT
FA	0.4332	0.4990	0.4962	2.1217	1.7150	-	121.92	13.67	West Blocton E, Aldrich	AL
SM	0.7262	0.0594	-1.0695	1.8642	2.2505	-	-	-	Valles Marineris, Mars	-

Sample numbers starting with F are for fluvial basins; those starting with S are for sapping basins. The last two samples are test samples from Alabama and Mars. The drainage density is based on a threshold flow accumulation area of 150 GRID cells [*Environmental Systems Research Institute*, 1993]. INT, hypsometric interval; SK, skewness of the hypsometric curve; DSK, skewness of hypsometric density function; KUR, kurtosis of the hypsometric curve; DKUR, kurtosis of the hypsometric density function; DD, drainage density in km^{-1}; Relief, elevation difference between summit and outlet in meters; Area, the area of the watershed basin in km^2. * indicates basins that were misclassified into the other group.

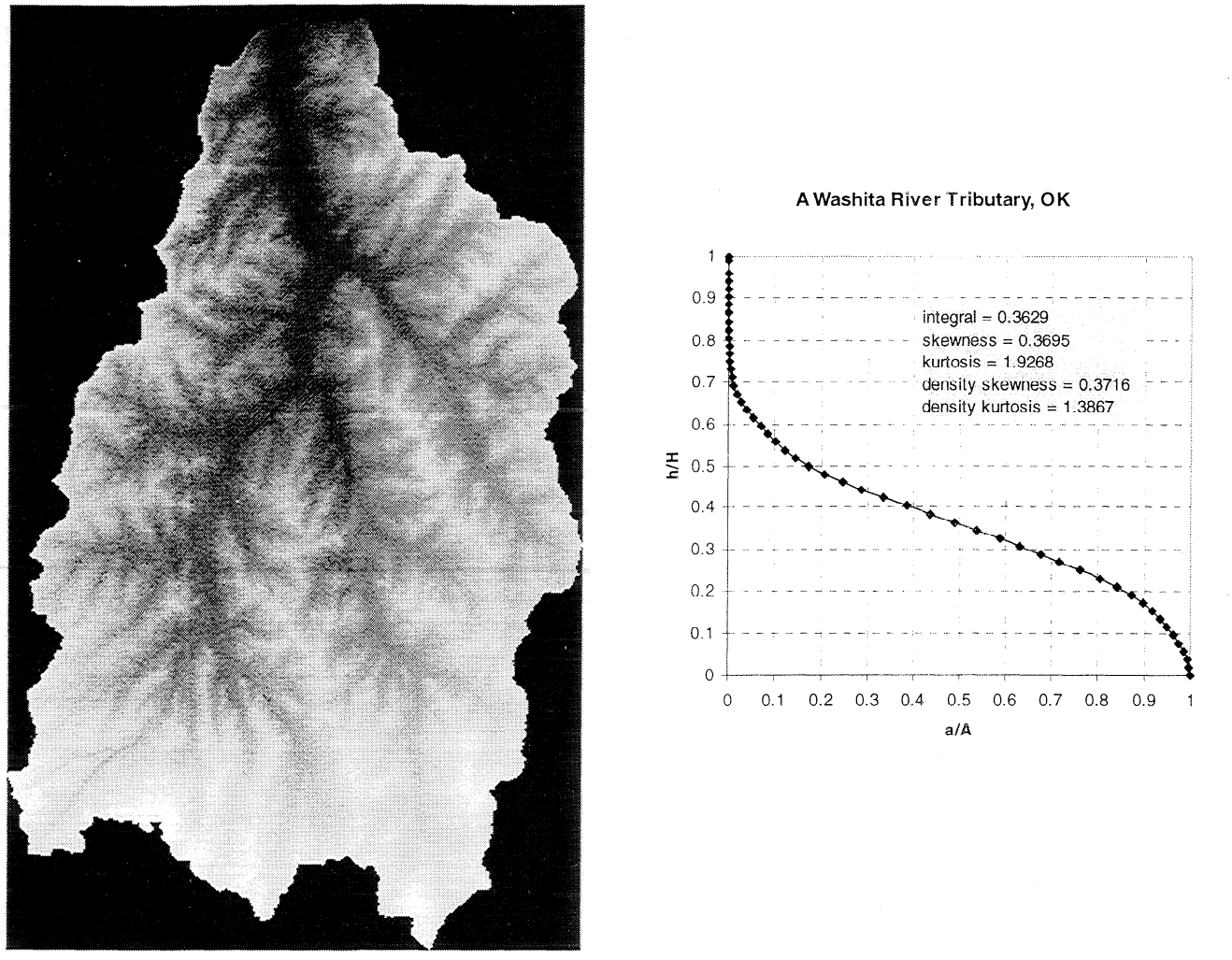

Figure 4. (a) Ditigal elevation model (DEM) of a typical fluvial landform (sample F6 in Table 1) and its hypsometric curve and attributes. The size of the DEM image is about 16.6 km × 10.1 km. The hypsometric curve is more concave upward in its middle to upper portion, indicating that there is little erosion at the lower reach and more erosion at the upper reach of the basin. (b) DEM of a typical sapping landform (sample S16 in Table 1) and its hypsometric curve and attributes. The dimensions of the DEM image are about 13 km × 5.8 km. The hypsometric curve is more convex upward in its middle to lower portion, indicating that there is more erosion at the lower reach of the basin and less erosion at the upper reach of the basin. North is toward the top.

$$F = -157.3274 + 98.9434 \times DSK + 536.7120 \times INT + 164.4041 \times SK, \quad (8)$$

$$S = -161.9439 + 93.3136 \times DSK + 551.2865 \times INT + 154.4376 \times SK, \quad (9)$$

where F is the linear discriminant function for a fluvial landform, S is the linear discriminant function for a sapping landform, DSK is skewness of the hypsometric density function, INT is the hypsometric interval, and SK is skewness of the hypsometric curve.

To help identify the possible origin of a basin based on its form, its hypsometric attributes are plugged into the above discriminant equations. It is possibly of sapping origin if $F>S$; it is possibly of fluvial origin if $S>F$. Other lines of evidence are needed to make a sure determination of the origin because the same form may be formed by different processes [*Dunne*, 1990]. Applying the above discriminant function back to the original samples that the discriminant function was derived from shows that most of the basins were separated correctly, except for two fluvial basins (out of 20) misclassified as sapping basins and one sapping basin (out of 25) misclassified as a fluvial basin (Table 1).

In order to test the effectiveness of the discriminant functions, two additional samples that did not participate in deriving the discriminant functions were collected from Alligator Creek, Alabama (FA in Table 1), and from Viking topographic data of Mars near the southwestern edge of Valles Marineris [*Higgins*, 1982] (SM in Table 1). The above discriminant functions identify SM as possibly sapping and FA as possibly fluvial on the basis of their hypsometric forms.

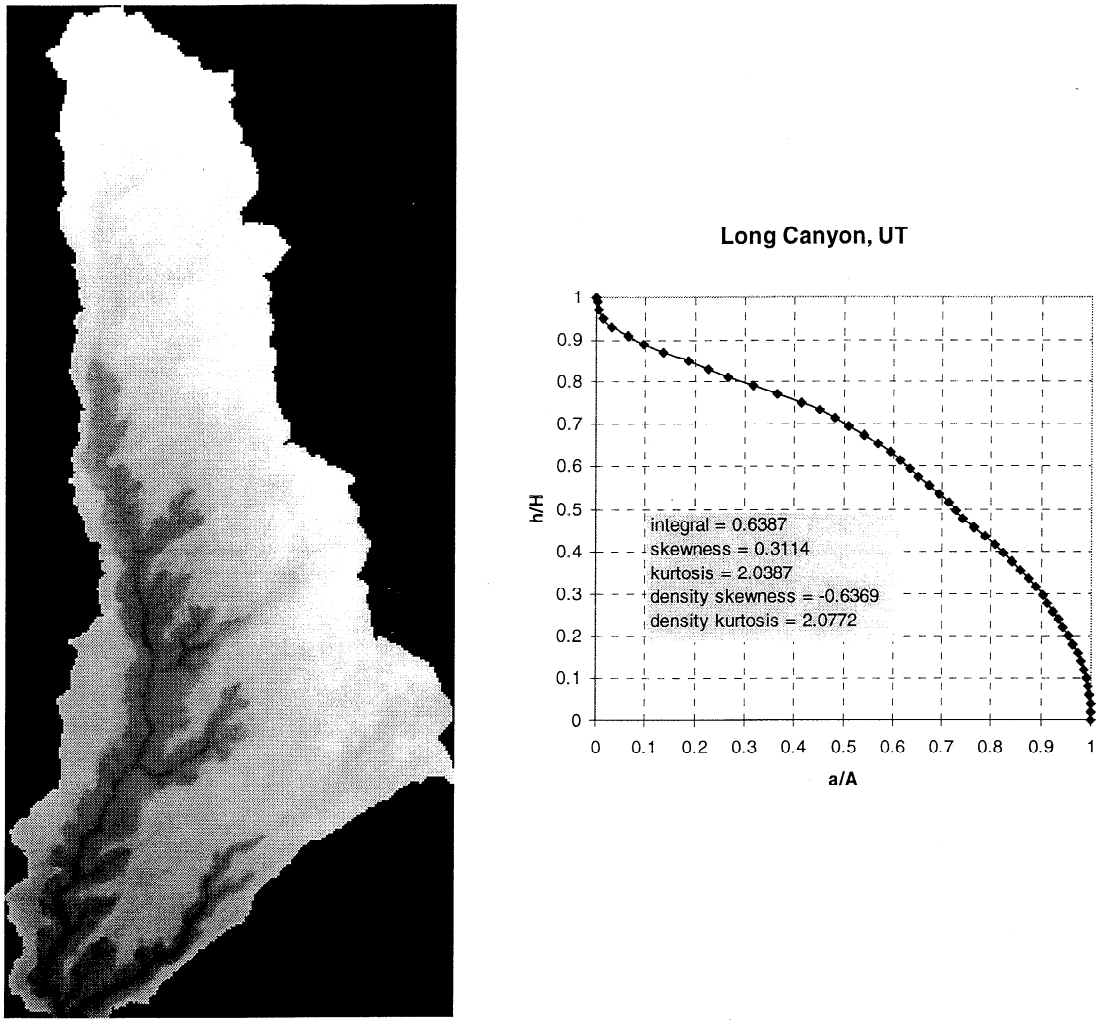

Figure 4. (continued)

5. Discussion

The above results indicate that the hypsometric technique does a reasonably good job in separating land forms that are characteristic of typical sapping and fluvial origins. However, these are the ideal end-member situations. This technique alone cannot offer a direct determination on the processes that are responsible for the forms because mixed processes and different processes could result in very similar forms [*Dunne*, 1990]. However, this technique can be used as a means to help identify the forms that might be caused by sapping or fluvial processes and to help quantitatively compare computer modeling results and reality. Other information and evidence (e.g., field work on Earth, rover exploration and computer modeling for Mars) are needed to make a more confident determination because the similar form may have resulted from different processes under different geologic settings [*Dunne*, 1990]. For example, sapping-looking forms could be generated by fluvial process in a geological setting that has resistant caprock strata and nickpoints, which inhibit fluvial dissection in the upper land; or they could be formed by plunge-pool recession.

Table 2. Statistical *t* Test Results

Variable	Mean		Standard Deviation		Prob>|T|	
	Fluvial	Sapping	Fluvial	Sapping	Unequal Variance	Equal Variance
INT	0.4465	0.5653	0.0641	0.0504	0.0001	0.0000
SK	0.3952	0.2938	0.0830	0.0548	0.0001	0.0000
KUR	2.0325	1.9794	0.0922	0.0679	0.0388	0.0315
DSK	0.1012	-0.3510	0.2048	0.2239	0.0001	0.0000
DKUR	1.4210	1.5961	0.0973	0.3384	0.0200	0.0305

See Tables 1 footnote for explanations of variables. Prob > |T| is the two-sided p value. The p values under both unequal variance and equal variance assumptions are listed.

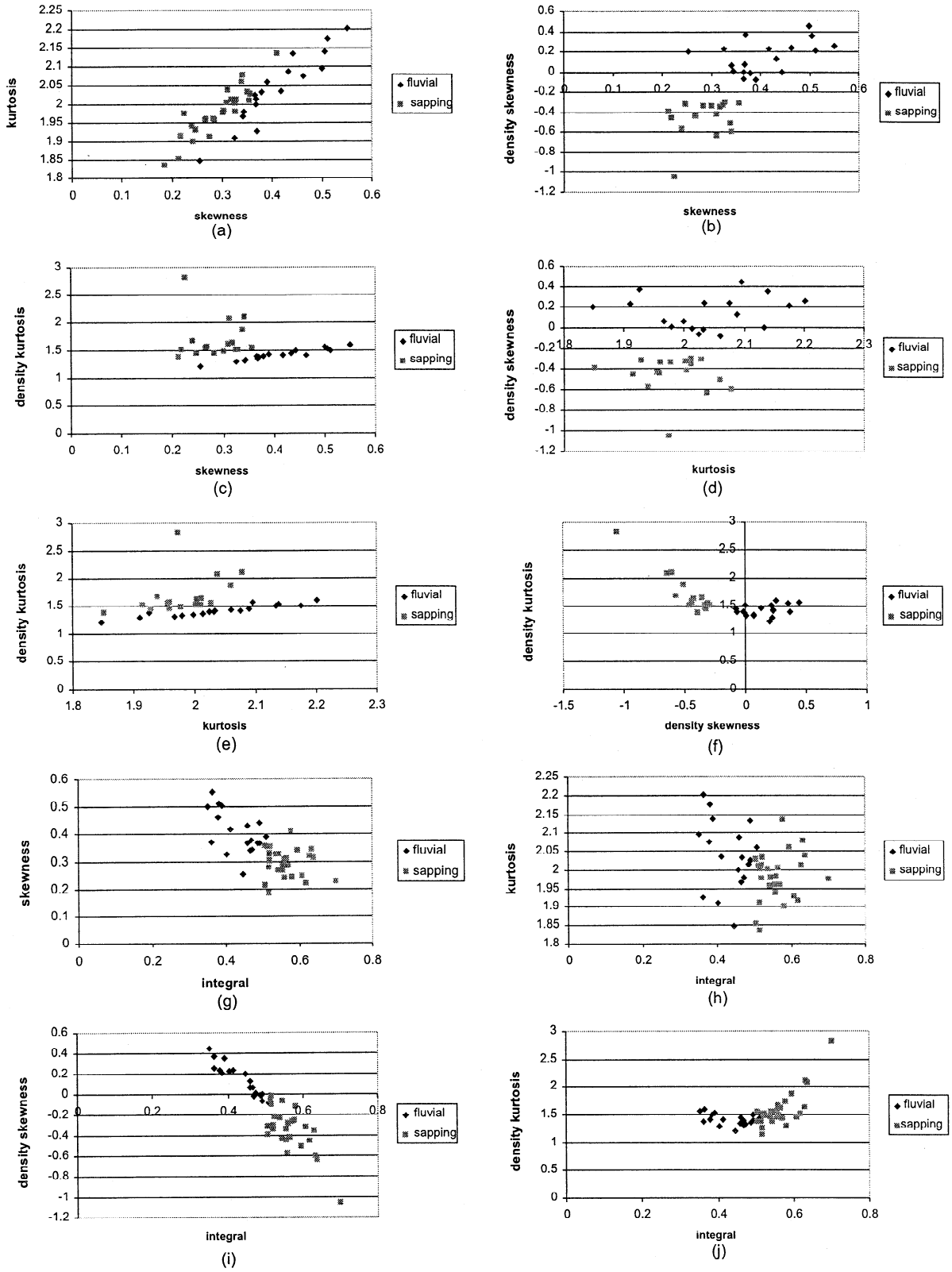

Figure 5. Scatterplots of all possible two-pair combinations of the five hypsometric attributes. The sapping and fluvial landforms can be readily separated by hypsometric attributes despite the overlap in value range in kurtosis and density kurtosis.

Table 3. Principal Component Analysis Results

Principal Component	Eigen-value	Variable Loading					% Total Variance	Cum. % Total Var.
		INT	SK	DSK	KUR	DKUR		
PRIN1	3.0137	-0.5327	0.4988	0.5354	0.3207	-0.2791	60.2738	60.2740
PRIN2	1.6696	0.1699	0.3835	-0.2364	0.6197	0.6198	33.3910	93.6650
PRIN3	0.2488	0.5414	0.0864	-0.1641	0.4325	-0.6968	4.9766	98.6410
PRIN4	0.0637	0.6080	0.0539	0.7492	-0.1339	0.2195	1.2742	99.9160
PRIN5	0.0042	0.1570	0.7705	-0.2630	-0.5552	-0.0651	0.0844	100.0000

See Tables 1 footnote for explanations of variables.

The three misclassifications by the discriminant functions suggest that even though the hypsometric technique does a reasonably good job in distinguishing landforms, we should not disregard the planform information such as drainage density, which is also valuable in identifying and separating forms characteristic of sapping and fluvial origins. Drainage density can be obtained from the DEM by using GRID functions in Arc/Info [*Environmental Systems Research Institute*, 1993]. Results show that the mean drainage density for the fluvial landform (1.826 km^{-1}) is higher than that of the sapping landform (1.734 km^{-1}) (DD in Table 1). The *t* test for drainage density (not shown) also indicates that it is significantly different between the two groups. However, adding drainage density to discriminant analysis results in the same error rate. Nonetheless, drainage densities for the misclassified fluvial basins are higher than that of the misclassified sapping basin (Table 1), consistent with expectation.

The misclassified fluvial basins (F2 and F19 in Table 1) are located in southwest Wisconsin and northwest Iowa, where some periglacial and mass-wasting processes may have occurred [*Bridges*, 1990] in the lower reaches of the basin, which makes the curve look like the groundwater-sapping landform (Figure 6). The misclassified sapping basin (S15 in Table 1) might have been further modified by surface fluvial processes, resulting in a low hypsometric integral and other

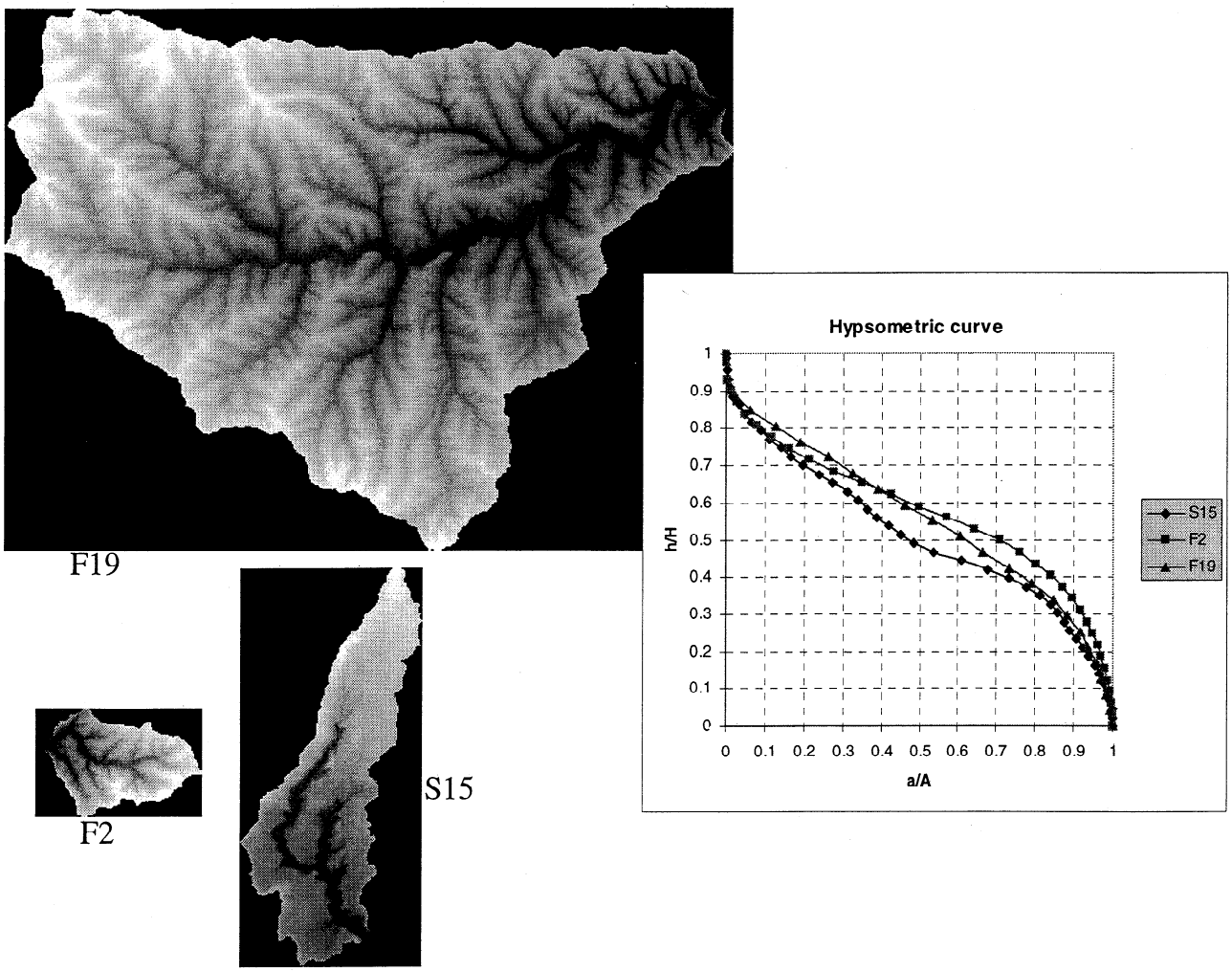

Figure 6. The DEMs of the misclassified basins and their hypsometric curve. See Table 1 for their hypsometric attributes and drainage density. The dimensions of the DEM image for F19 is 12.1 km × 16.3 km; F2 dimensions are 2.4 km × 3.7 km; and S15 dimensions are 8.9 km × 4.1 km. North is toward the top.

attributes more fluvial-like (Figure 6). Other factors such as lithology, structure, climate, and stage of landform development should be investigated further to explain the error and to make a more confident determination of their origins. Nonetheless, the hypsometric technique provided at least an alternative means to quantify landforms. It has promise for testing hypotheses for the origin of landforms on other planets such as Mars, and it should be used in conjunction with other planform parameters, such as drainage density, to describe the landform more fully and with other lines of evidence, such as field work and computer modeling, to assign the process responsible for the form.

6. Conclusion

In conclusion, the hypsometric technique provided an alternative means to quantify landforms, and it is now practical to apply this technique to digital data within a GIS environment. This paper showed that the hypsometric attributes did a reasonably good job in separating typical sapping and fluvial landforms on Earth on the basis of their forms. Of the five hypsometric attributes, density skewness, hypsometric integral, and skewness seem to be particularly powerful in separating the two landforms. The hypsometric technique should probably be used in conjunction with other planform parameters and other evidence and information (field work, computer modeling, etc.) to determine the process responsible for the form. This technique can be used to quantify landforms and to help explore and identify the origin of landforms on other planets such as Mars, where groundwater-sapping is thought to have played an important role in its landform evolution. Thus this technique could also be helpful in selecting future landing sites on Mars.

Acknowledgements. I would like to thank John M. Harlin for introducing me the hypsometric technique and for his encouragement during this project. The careful reviews by Victor R. Baker and Thomas Dunne and an anonymous reviewer of an earlier version of this paper helped to improve the quality of this paper and are greatly appreciated. Thanks to Leonard A. Walther for redrawing Figure 1.

References

Baker, V. R., *The Channels of Mars*, 198 pp., Univ. of Tex. Press, Austin, 1982.

Bridges, E. M., *World Geomorphology*, pp. 84-87, Cambridge Univ. Press, New York, 1990.

Carr, M. H., Global history of water and climate, paper presented at Fifth International Conference on Mars, California Institute of Technology, Pasadena, Calif. July 18-23, 1999.

Coates, D. R., The relation of subsurface water to downslope movement and failure, in *Groundwater Geomorphology: The Role of Subsurface Water in Earth-Surface Processes and Landforms*, edited by C. G. Higgins and D. R. Coates, *Spec. Pap. Geol. Soc. Am., 252*, 51-76, 1990.

Coradini, M., M. Fulchignoni, and F. Visicchio, The hypsometric curve of Mars, *The Moon and the Planets*, 22, 201-210, 1980.

Dunne, T. Hydrology, mechanics, and geomorphic implications of erosion by subsurface flow, in *Groundwater Geomorphology: The Role of Subsurface Water in Earth-Surface Processes and Landforms*, edited by C. G. Higgins and D. R. Coates, *Spec. Pap. Geol. Soc. Am., 252*, 1-28, 1990.

Environmental Systems Research Institute, Understanding GIS: The Arc/Info Method, version 6 for workstations, Redlands, Calif., 1993.

Gulick, V. C., Magmatic intrusions and a hydrothermal origin for fluvial valleys on Mars, *J. Geophys. Res*, *103*(8), 19,365-19,387, 1998.

Gulick, V. C., and V. R. Baker, Fluvial valleys and Martian palaeoclimates, *Nature*, *341* (6242), p. 514-516, 1989.

Gulick, V. C., and V. R. Baker, Origin and evolution of valleys on Martian volcanoes, *J. Geophys. Res.*, *95*(9), 14,325-14,344, 1990.

Harlin, J. M., Statistical moments of the hypsometric curve and its density function, *J. Int. Assoc. Math. Geol.*, *10*, 59-72, 1978.

Harlin, J. M., Geology and geomorphology of the southern plains research watershed, *Okla. Geol. Notes*, *42*, 168-178, 1982.

Harlin, J. M., Watershed morphometry and time to hydrograph peak, *J. Hydrol.*, *67*, 141-154, 1984.

Higgins, C. G., Drainage systems developed by sapping on Earth and Mars, *Geology*, *10*, 147-152, 1982.

Higgins, C. G., Piping and sapping: Development of landforms by groundwater outflow, in *Groundwater as a Geologic Agent*, edited by R. G. LaFleur, pp. 18-58, Allen and Unwin, Boston, Mass., 1984.

Higgins, C. G. and D. R. Coates, (Eds.), *Groundwater Geomrophology; The Role of Subsurface Water in Earth-Surface Processes and Landforms*, *Spec. Pap. Geol. Soc. Am., 252*, 368 pp., 1990.

Howard, A. D., Groundwater-sapping experiments and modeling, in *Sapping Features of the Colorado Plateau, A Comparative Planetary Geology Field Guide*, *NASA SP-491*, 71-83, 1988.

Howard, A. D., R. C. Kochel, and H. E. Holt, *Sapping Features of the Colorado Plateau, A Comparative Planetary Geology Field Guide*, *NASA SP-491*, 107 pp., 1988.

Jones, J. A. A., Subsurface flow and subsurface erosion – Further evidence on forms and controls, in *Process and Form in Geomorphology*, edited by D. R. Stoddart, pp. 74-120, Routledge, New York, 1997.

Kochel, R. C., and J. F. Piper, Morphology of large valleys on Hawaii: Evidence for groundwater sapping and comparisons with Martian valleys, *J. Geophys. Res.*, *91*, e175-e192, 1986.

Laity, J. E., and M. C. Malin, Sapping processes and the development of theater-headed valley networks on the Colorado Plateau, *Geol. Soc. Am. Bull.*, *96*, 203-217, 1985

Lane, S. N., J. H. Chandler, and K. S. Richards, Landform monitoring, modeling, and analysis: Land form in geomorphological research, in *Landorm Monitoring, Modeling and Analysis*, edited by S. N, Lane, K. S. Richards, and J. H., Chandler, John Wiley, New York, pp.1-18, 1998,

Langbein, W. B., Topographic characteristics of drainage basin, *U. S. Geol. Surv. Water Supply Pap., 968-C*, 125-157, 1947.

Luo, W., Hypsometric analysis with Geographic Information System (GIS), *Comput. Geosc.*, *24*, 815-821, 1998.

Luo, W., R. E. Arvidson, M. Sultan, R. Becker, M. K. Crombie, N. Sturchio, and Z. E. Alfy, Ground-water sapping process, Western Desert, Egypt, *Geol. Soc. Am. Bull.*, *109*, 43-62, 1997.

Malin, M. C., and M. H. Carr, Groundwater formation of Martian valleys, *Nature*, *397*(6720), 589-591, 1999.

Nash, D. J., Groundwater-sapping and valley development in the Hackness Hills, North Yorkshire, England, *Earth Surf. Processes Landforms*, *21*, 781-795, 1996.

Onda, Y., Seepage erosion and its implication to the formation of amphitheartre valley heads, A case study at Obara, Japan, *Earth Surf. Processes Landforms*, *19*, 627-640, 1994.

SAS Institute Inc., *SAS/STAT User's Guide, Version 6*, 4th ed., Gary, N.C., 1990.

Schumm, S. A., K. F. Boyd, C. G. Wolff, and W. J. Spitz, A ground-water sapping landscape in the Florida Panhandle, *Geomorphology*, *12*, 281-297, 1995.

Squyres, S. W., and J. F. Kasting, Early Mars: How warm and how wet?, *Science*, *265*, 744- 749, 1994.

Strahler, A. N., Hypsometric (area-altitude) analysis of erosional topography, *Geol. Soc. Am. Bull.*, *63*, 1117-1142, 1952.

Uchupi, E., and R. N. Oldale, Spring sapping origin of the enigmatic relict valleys of Cape Cod and Martha's Vineyard and Natucket Islands, Massachusetts, *Geomorphology*, *9*, 83-95, 1994.

W. Luo, Department of Geography, Northern Illinois Univeristy, DeKalb, IL 60115-2854. (luo@geog.niu.edu)

(Received May 27, 1999; revised October 25, 1999;
accepted November 1, 1999.)